Available online at www.sciencedirect.com
SCIENCE DIRECT®
Combustion and Flame 137 (2004) 489–505
Combustion and Flame
www.elsevier.com/locate/jnlabr/cnf

Compressible large eddy simulation of turbulent combustion in complex geometry on unstructured meshes

L. Selle,[a,*] G. Lartigue,[a] T. Poinsot,[b] R. Koch,[c] K.-U. Schildmacher,[c] W. Krebs,[d] B. Prade,[d] P. Kaufmann,[d] and D. Veynante [e]

[a] *CERFACS, CFD team, 42 Av. G. Coriolis, 31057 Toulouse Cedex, France*
[b] *IMF Toulouse, UMR CNRS/INP-UPS 5502, Allée du Pr. C. Soula, 31400 Toulouse Cedex, France*
[c] *Institute of Thermal Turbomachinery, University of Karlsruhe, Kaiserstrasse 12, 76128 Karlsruhe, Germany*
[d] *Siemens PG, Muelheim, Germany*
[e] *Laboratoire EM2C, Ecole Centrale de Paris and CNRS, 92295 Châtenay Malabry Cedex, France*

Received 20 June 2003; received in revised form 5 March 2004; accepted 18 March 2004

Available online 13 April 2004

Abstract

Large-eddy simulations (LESs) of an industrial gas turbine burner are carried out for both nonreacting and reacting flow using a compressible unstructured solver. Results are compared with experimental data in terms of axial and azimuthal velocities (mean and RMS), averaged temperature, and existence of natural instabilities such as precessing vortex core (PVC). The LES is performed with a reduced two-step mechanism for methane–air combustion and a thickened flame model. The regime of combustion is partially premixed and the computation includes part of the swirler vanes. For this very complex geometry, results demonstrate the capacity of the LES to predict the mean flow, with and without combustion, as well as its main unstable modes: it is shown, for example, that the PVC mode is very strong for the cold flow but disappears with combustion.

Keywords: Large-eddy simulation; Combustion; Complex geometries

1. Introduction

Large-eddy simulation (LES) is becoming a standard tool to study the dynamics of turbulent flames [1,2]. Multiple recent papers have demonstrated the power of this method [3–9]. For example, LES appears as one of the key tools to predict and study combustion instabilities encountered in many modern combustion devices such as aero and industrial gas turbines, rocket engines, and industrial furnaces.

Up to now, most LES of reacting flows has been limited to fairly simple geometries for obvious reasons of cost and complexity reduction. In many cases, experiments have been designed using especially simple shapes (two-dimensional [3,7,10] or axisymmetrical [11,12] configurations) and simple regimes (low-speed flows, fully premixed or fully non-premixed flames) to allow research to focus on the physics of the LES (subgrid scale models, flame/turbulence interaction model) and, more generally, to demonstrate the validity of the LES concept in academic cases. Even though this approach is clearly adequate in terms of model development, it is important to recognize that it can also be misleading in various aspects when it comes to dealing with complex flames in complex geometries:

- Most LES of reacting flows have been performed in combustion chambers where structured meshes were sufficient to describe the geometry. In such solvers, using high-order spa-

* Corresponding author. Fax: 33-561-193-000.
E-mail address: selle@cerfacs.fr (L. Selle).

0010-2180/$ – see front matter
doi:10.1016/j.combustflame.2004.03.008

tial schemes (typically fourth to sixth order in space) is relatively easy and provides precise numerical methods. As soon as real complex geometries are considered, these structured meshes must be replaced by unstructured grids on which constructing high-order schemes is a much more difficult task.

- Moving from structured to unstructured meshes also raises a variety of new problems in terms of subgrid scale filtering: defining filter sizes on a highly anisotropic irregular grid is another open research issue [13–16]. Many LES models, developed and tuned on regular hexahedral grids, perform much more poorly on the irregular unstructured grids required to mesh real combustion chambers. Very few studies have been published yet on LES of reacting flows on unstructured grids [4,5,17]. One objective of this article is to demonstrate the ability of a present LES tool to handle such meshes.
- Many laboratory flames used for LES validations are low-speed unconfined flames in which acoustics do not play a role and the Mach number remains small so that compressibility effects can be omitted from the equations (so-called "low-Mach-number approximation"). In most real flames (e.g., in gas turbines), however, compressibility cannot be neglected: (1) the Mach number can reach much higher values, and (2) acoustics are important so that taking into account compressibility effects becomes mandatory. This leads to a more complex formulation in which the boundary conditions must handle acoustic wave reflections [2]. Being able to preserve computational speed on a large number of processors then also becomes an issue simply to obtain a result in a finite time.
- In many combustion chambers, it is impossible to perform true LES everywhere in the flow. For example, the flow between vanes in swirled burners or inside the ducts feeding dilution jets would require too many grid points. Multiperforated plates, which can create thousands of small jets cooling the combustion chamber, are also obviously beyond the present capabilities of LES codes. As a consequence, compromises must be sought and the LES of today and probably tomorrow requires methods that offer (at least) robustness in places where the grid is not sufficient to resolve the unsteady flow. For such methods, having excellent LES efficiency on high-quality grids for academic problems is no longer the most important issue.

These few examples suggest that when it comes to computing flames in complex geometries for real combustors, work must concentrate on new issues: unstructured solvers, compressible flows, boundary conditions, robustness in poorly meshed zones, parallel efficiency. This also means that many modeling aspects that were critical in simple laboratory flames (subgrid scale LES models for momentum, kinetic energy conservation, accuracy of chemistry description, etc.) must now be combined with other (and sometimes more) critical problems: efficient unstructured solvers, subgrid scale LES models on distorted grids, boundary conditions adapted to acoustics, etc.

The choice of a chemistry description remains a significant difficulty. For most laboratory flames, describing chemistry with only one variable is sufficient for LES: the progress variable is enough to compute fully premixed flames and the mixture fraction is adequate for perfectly non-premixed piloted flames such as the Sandia flames [18]. In real gas turbines however, the combustion regime is much more complex and more "robust" models are required to handle flames that are typically partially premixed with a full range of local equivalence ratios and mixing levels.

This study presents a computation of a complex industrial burner, developed at Siemens Power Generation, using an unstructured LES compressible solver. The main objectives are to:

- extend an existing flame/interaction model (called the Thickened Flame Model) to a two-step chemical scheme,
- investigate the capabilities of LES in a realistic configuration, and
- compare the LES results with experimental data obtained at the University of Karlsruhe. This comparison is performed for one regime only for which detailed LES and experimental results are gathered. This regime corresponds to a partially premixed case at an equivalence ratio of $\phi = 0.5$ and an inlet temperature of 673 K. This regime does not exhibit large-scale combustion instabilities.

The LES solver used for the study is presented first. The Thickened Flame (TF) model is then discussed. A two-step chemical mechanism incorporating CO as the main intermediate species was tuned for the conditions of the Siemens burner and tested first for premixed laminar flames. The configuration used for the Siemens burner installed in the Karlsruhe combustion chamber is described before presenting cold flow results. Finally, reacting flow solutions are presented. For both reacting and nonreacting cases, the presentation includes a comparison of the averaged fields (mean and RMS velocities for all cases, temperature for the reacting case) and a study of the precessing vortex core.

2. The LES solver

The LES solver AVBP [19] solves the full compressible Navier–Stokes equations on hybrid (structured and unstructured) grids. Subgrid stresses are described by the WALE model [20]. The flame/turbulence interaction is modeled by the TF approach [3,5,7,21,22]. The numerical scheme uses third-order spatial accuracy and third-order time accuracy [23]. Tests performed during this study have demonstrated that the third-order spatial accuracy of the solver is a key feature in obtaining precise LES results on unstructured meshes. The AVBP solver used here also handles variable heat capacities: species enthalpies are tabulated and the mean heat capacity is determined as a function of temperature and species mass fractions Y_k. Therefore, local quantities, such as the mean molar mass W and the ratio of heat capacities γ, are not constant. This introduces significant additional complexities into the numerical method, especially near boundaries where classic characteristic methods such as NSCBC [24] must be replaced by a more complex technique [25]. The walls of the combustion chamber are treated as adiabatic walls (the experiment uses ceramic walls). Both no-slip and law-of-the-wall formulations have been used on walls, with very limited differences in the results. Typical runs are performed on grids of 2.5 millions elements on 64 processors.

3. The thickened flame model

For the present study, premixed combustion is considered. Multiple studies have concentrated on LES of diffusion flames [8,26,27] while premixed cases have received less attention [9,28–30]. Indeed, infinitely fast chemistry assumptions constitute a useful path for LES of diffusion flames. Such assumptions cannot be used for premixed flames, however: modeling the interaction between flame and turbulence in premixed combustion systems requires tracking of the flame front position, leading to a problem that is more difficult to handle than most diffusion flames. The natural technique to track the flame would be to solve its inner structure, but this is impossible on typical LES meshes because premixed flame fronts are too thin. Two methods can then be used to propagate turbulent flame fronts on LES meshes:

- Bring the flame thickness to zero and propagate the flame front as a thin interface: this is the principle of the G-equation method [1,9].
- Thicken the flame so that it can be resolved on the LES mesh while still propagating at the same speed as the unthickened flame: this is the principle of the TF model [2,5].

In the present work, the standard TF model developed by Colin et al. [5] is used: in this model, preexponential constants and transport coefficients are both modified to offer thicker reaction zones that can be resolved on LES meshes. The fundamental property justifying this approach has been put forward by Butler and O'Rourke [31] by considering the balance equation for the k-species mass fraction Y_k in a one-dimensional flame of thermal thickness δ_{L}^0 and speed s_{L}^0:

$$\frac{\partial \rho Y_k}{\partial t} + \frac{\partial \rho u Y_k}{\partial x} = \frac{\partial}{\partial x}\left(\rho D_k \frac{\partial Y_k}{\partial x}\right) + \dot{\omega}_k(Y_j, T). \tag{1}$$

Modifying this equation to have

$$\frac{\partial \rho Y_k^{\mathrm{th}}}{\partial t} + \frac{\partial \rho u Y_k^{\mathrm{th}}}{\partial x} = \frac{\partial}{\partial x}\left(\rho F D_k \frac{\partial Y_k^{\mathrm{th}}}{\partial x}\right) + \frac{1}{F}\dot{\omega}_k\left(Y_j^{\mathrm{th}}, T^{\mathrm{th}}\right) \tag{2}$$

leads to a "thickened" flame equation where F is the thickening factor and superscript th stands for thickened quantities. Introducing the variable changes $X = x/F$ and $\Theta = t/F$ leads to:

$$\frac{\partial \rho Y_k^{\mathrm{th}}}{\partial \Theta} + \frac{\partial \rho u Y_k^{\mathrm{th}}}{\partial X} = \frac{\partial}{\partial X}\left(\rho D_k \frac{\partial Y_k^{\mathrm{th}}}{\partial X}\right) + \dot{\omega}_k\left(Y_j^{\mathrm{th}}, T^{\mathrm{th}}\right), \tag{3}$$

which has the same solution as Eq. (1) and propagates the flame front at the same speed s_L^0. However, $Y_k^{\mathrm{th}}(x,t) = Y_k(x/F, t/F)$, showing that the flame is thickened by a factor F. The thickened flame thickness is $\delta_{\mathrm{L}}^1 = F\delta_{\mathrm{L}}^0$. Choosing sufficiently large values of F allows us to obtain a thickened flame that can be resolved on the LES mesh. Typically, if n is the number of mesh points within the flame front required by the solver and Δx the mesh size, the resolved flame thickness δ_{L}^1 is $n\Delta x$, so that F must be $F = n\Delta x/\delta_{\mathrm{L}}^0$. For the computation of most flames using the TF model, values of F ranging from 5 to 50 are sufficient to resolve the flame front on meshes corresponding to present computer capabilities. In the framework of LES, this approach has multiple advantages: when the flame is a laminar premixed front, the TF model propagates it at the laminar flame speed exactly as in a G equation approach [1]. However, this flame propagation is due to the combination of diffusive and reactive terms which can also act independently so that quenching (near walls for example) or ignition may be simulated. Fully compressible equations may also be used as required to study combustion instabilities.

Obviously, thickening the flame front also leads to a modified interaction between the turbulent flow and the flame: subgrid scale wrinkling must be reintroduced. This effect can be studied and parametrized using an efficiency function E derived from DNS results [5,21,32]. This efficiency function measures the subgrid scale wrinkling as a function of the local subgrid turbulent velocity u'_{Δ_e} and the filter width Δ_e. In practice, the diffusion coefficient D_k is replaced by EFD_k and the preexponential constant A by AE/F so that the conservation equation for species k is

$$\frac{\partial \rho Y_k^{\mathrm{th}}}{\partial t} + \frac{\partial \rho u Y_k^{\mathrm{th}}}{\partial x} = \frac{\partial}{\partial x}\left(\rho EFD_k \frac{\partial Y_k^{\mathrm{th}}}{\partial x}\right) + \frac{E}{F}\dot{\omega}_k\left(Y_j^{\mathrm{th}}, T^{\mathrm{th}}\right). \quad (4)$$

This equation allows the turbulent flame to propagate at a turbulent speed $s_T = Es_L^0$ while keeping a thickness of the order of $\delta_L^1 = F\delta_L^0$. In laminar regions, E goes to unity and Eq. (4) simply propagates the front at the laminar flame speed s_L^0.

A central ingredient of the TF model is the subgrid scale wrinkling function E. For this work, the initial model of Colin et al. [5] was used to express E as a function of the local filter size Δ_e, the local subgrid scale turbulent velocity u'_{Δ_e}, the laminar flame speed s_L^0, and the laminar flame thicknesses δ_L^0 and δ_L^1,

$$E = \frac{\Xi(\delta_L^0)}{\Xi(\delta_L^1)} = \left(1 + \alpha\Gamma\left(\frac{\Delta_e}{\delta_L^0}, \frac{u'_{\Delta_e}}{s_L^0}\right)\frac{u'_{\Delta_e}}{s_L^0}\right) \times \left(1 + \alpha\Gamma\left(\frac{\Delta_e}{\delta_L^1}, \frac{u'_{\Delta_e}}{s_L^0}\right)\frac{u'_{\Delta_e}}{s_L^0}\right)^{-1}, \quad (5)$$

where the function Γ corresponds to the integration of the effective strain rate induced by all scales affected by the artificial thickening, i.e., between the Kolmogorov η_K and the filter Δ_e scales. α is a model parameter that scales as $\alpha \propto Re^{-1/2}$ [5]. Γ is written as:

$$\Gamma\left(\frac{\Delta_e}{\delta_L^1}, \frac{u'_{\Delta_e}}{s_L^0}\right) = 0.75\exp\left[-\frac{1.2}{(u'_{\Delta_e}/s_L^0)^{0.3}}\right]\left(\frac{\Delta_e}{\delta_L^1}\right)^{2/3}. \quad (6)$$

The subgrid scale turbulent velocity is evaluated as $u'_{\Delta_e} = 2\Delta_x^3|\nabla^2(\nabla \times \vec{u})|$, where Δ_x is the grid size. This formulation provides an estimate of the subgrid scale velocity which is unaffected by dilatation [5]. Note that the filter size Δ_e may differ from Δ_x. Colin et al. [5] suggested choosing $\Delta_e = 10\Delta_x$.

The LES studies of Angelberger et al. [3] and Colin et al. [5] as well as various other tests have shown that Eq. (5) is adequate in predicting subgrid scale wrinkling. In this work, a thickening factor $F = 25$ was used. Eq. (5) was developed and tested with single-step chemical schemes. As the present study uses a two-step mechanism, additional DNS were performed to study the TF approach combined with a two-step chemical scheme [33] and to check whether the existing efficiency functions proposed in [5,21] or [32] could be used without modification. Results showed that the two chemical reaction rates follow exactly the same evolution during these flame vortex interactions. These DNS suggest that, for the investigated range of parameters, the premixed flame acts as a flamelet distorted by flow motions even for low values of the length scale ratio $r/(F\delta_L^0)$, where r is the length scale on the vortices interacting with the flame front. Moreover, the effective strain rates induced by the vortices on the flame front and extracted from these DNS are in close agreement with [5,21] findings. Accordingly, the efficiency functions derived in [5,21,32] were used without any modifications with the present two-step chemical scheme.

4. Two-step chemistry

The complexity of the chemical scheme used in a TF model must remain limited because all species are explicitly resolved. Up to now, only simple one-step chemical schemes have been used in TF models [3,5]. In the present study, a two-step scheme is introduced to capture CO and predict more adequate flame temperatures as an intermediate step toward more complex schemes (typically four-step schemes such as [34]).

The chemical scheme (called 2sCM2) takes into account six species (CH_4, O_2, CO_2, CO, H_2O, and N_2) and two reactions:

$$CH_4 + \frac{3}{2}O_2 \rightarrow CO + 2H_2O, \quad (7)$$

$$CO + \frac{1}{2}O_2 \leftrightarrow CO_2. \quad (8)$$

The first reaction (7) is irreversible, whereas the second one (8) is reversible and leads to an equilibrium between CO and CO_2 in the burnt gases. The rates of reaction (7) and (8) are respectively given by

$$q_1 = A_1\left(\frac{\rho Y_{CH_4}}{W_{CH_4}}\right)^{n_1^{CH_4}}\left(\frac{\rho Y_{O_2}}{W_{O_2}}\right)^{n_1^{O_2}} \times \exp\left(-\frac{E_{a_1}}{RT}\right), \quad (9)$$

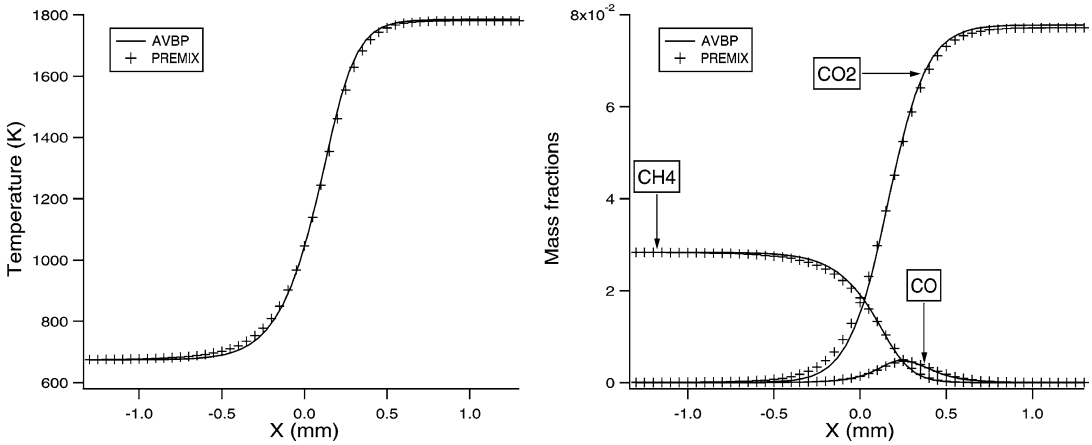

Fig. 1. Laminar one-dimensional flame at $\phi = 0.5$. Comparison of flame structures in AVBP and PREMIX with reduced scheme (called 2sCM2). (Left) Temperature profile (the fresh-gas temperature is 673 K), (right) mass fractions.

Table 1
Rate constants for the 2sCM2 scheme[a]

A_1	$n_1^{CH_4}$	$n_1^{O_2}$	E_{a_1}	A_2	n_2^{CO}	$n_2^{O_2}$	$n_2^{CO_2}$	E_{a_2}
$2E15$	0.9	1.1	34500	$2E9$	1	0.5	1	12000

[a] Activation energies are in cal/mol and the preexponential constants in cgs units.

Table 2
Schmidt numbers

CH_4	CO_2	CO	O_2	H_2O	N_2
0.68	0.98	0.76	0.76	0.6	0.75

$$q_2 = A_2\left[\left(\frac{\rho Y_{CO}}{W_{CO}}\right)^{n_2^{CO}}\left(\frac{\rho Y_{O_2}}{W_{O_2}}\right)^{n_2^{O_2}} - \frac{1}{K_e}\left(\frac{\rho Y_{CO_2}}{W_{CO_2}}\right)^{n_2^{CO_2}}\right] \times \exp\left(-\frac{E_{a_2}}{RT}\right), \quad (10)$$

where K_e is the equilibrium constant for reaction (8), and the other parameters are provided in Table 1.

Transport by molecular diffusion also requires attention: laminar flame codes such as PREMIX use polynomial fits for diffusion coefficients D_k. This technique is precise but expensive and may be replaced by a simpler approximation based on the observation that the individual Schmidt numbers of species $S_c^k = \nu/D_k$ are almost constant in many air/hydrocarbon flames. Therefore, in AVBP, the diffusion coefficient D_k of species k is obtained as $D_k = \nu/S_c^k$, where ν is the viscosity and S_c^k the fixed Schmidt number of species k. The Schmidt number values used in the present simulations are given in Table 2. In most cases, these values correspond to the PREMIX values measured in the burnt gases. The Prandtl number is set to 0.68. With this parameter set, the agreement between flame profiles obtained using AVBP or PREMIX with the same chemical scheme is excellent (Fig. 1).

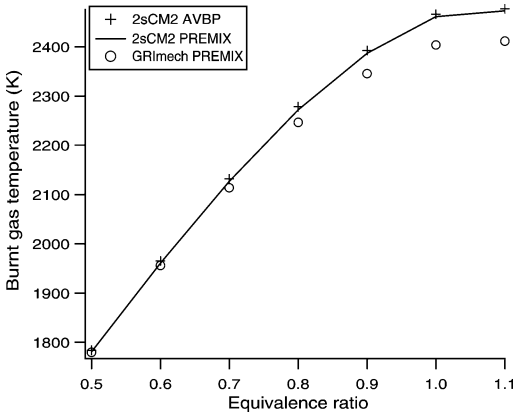

Fig. 2. Comparison of AVBP and PREMIX for burnt gas temperature (K). AVBP with reduced scheme (2sCM2) is compared with PREMIX results using both reduced and complex (GRI-Mech) schemes.

This scheme is directly implemented into the LES code. Its first advantage compared with a single-step scheme is to provide more accurate adiabatic flame temperatures. Fig. 2 compares the maximum flame temperatures obtained with AVBP and PREMIX using the full GRI mechanism. For the reduced scheme 2sCM2, AVBP and PREMIX predict the same maximum flame temperature, confirming that the thermodynamical data of AVBP are correct. The reduced scheme 2sCM2 overestimates the maximum flame temperatures compared with the GRI-mech scheme by 100 K for rich cases, but is very accurate for lean mixtures. The laminar flame speeds

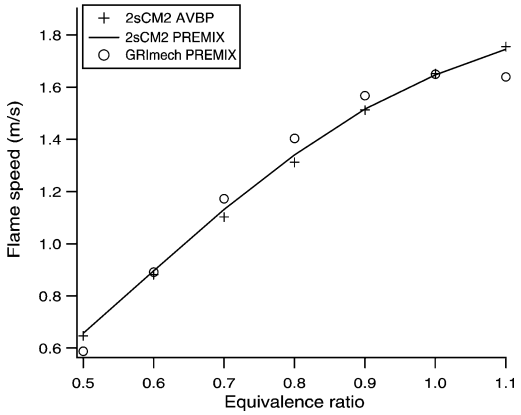

Fig. 3. Comparison of AVBP (reduced scheme 2sCM2) and PREMIX (reduced and complex schemes) for laminar flame speed s_L^0 (m/s).

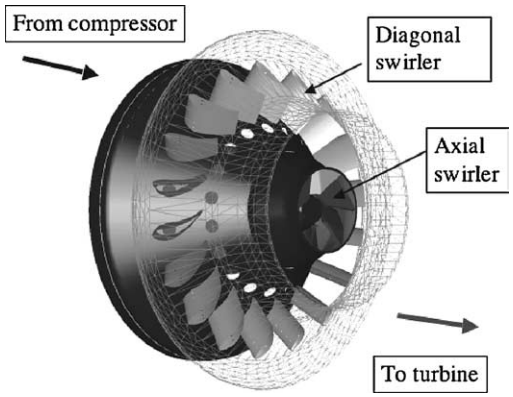

Fig. 4. View of the Siemens burner: the vanes of the diagonal swirler are not computed.

are also well predicted on the lean side (Fig. 3) but deviate from the exact results for rich cases. For the turbulent case presented below, the equivalence ratio varies between 0 and 0.5 so that the 2sCM2 predictions are precise.

5. Configuration

An important objective of this study is to investigate the limits of present computer capabilities to perform LES of combustion in realistic geometries. An industrial gas turbine burner is considered here. The CAD data were provided by Siemens PG. The grid contains 2,381,238 cells. Fig. 4 shows the main features of the burner. A central axial swirler (colored in dark) is used to inject and swirl air. This swirler is entirely computed in the LES. In addition, six small tubes (not visible on this figure) can be used to generate pilot flames in the axial swirler but they were not fed during the present computation. The main part of the combustion air is injected by the diagonal swirler. The fuel is injected in the diagonal swirler through holes located on both sides of the swirling vanes. The diagonal swirler vanes can be seen in Fig. 4. In this study, the flow produced by the diagonal swirler is assumed to be perfectly premixed and the computational domain starts at the trailing edge of the vanes.

6. Experimental techniques

A single Siemens burner (scale 1 : 1) is mounted on an atmospheric test rig (Fig. 5). The combustion

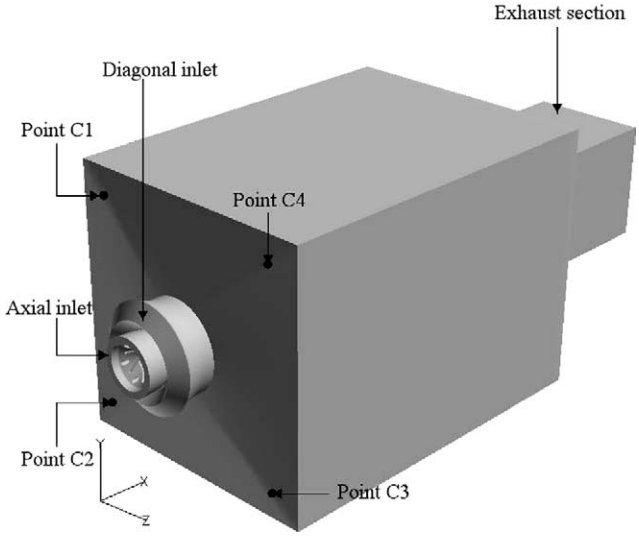

Fig. 5. Burner mounted on ITS combustion chamber.

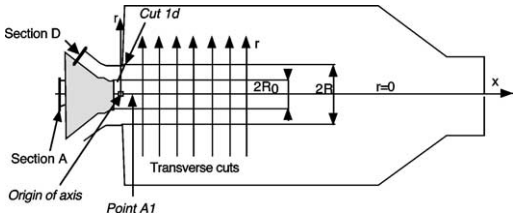

Fig. 6. Longitudinal cut of the combustion chamber: location of LDV measurements.

chamber has a square cross section with a truncated pyramid shape at the exit. Both the casing and the chamber walls allow optical access for velocity measurements by LDA. The burner is fired with natural gas (assumed to be mostly methane), and the air is preheated to 673 K. The thermal power varies between 420 kW (at $\Phi = 0.5$) and 810 kW (at $\Phi = 0.83$).

Measurements were performed at ITS Karlsruhe to characterize:

- the cold flow velocity field in terms of mean and RMS velocities using LDA techniques,
- the hot flow velocity field in terms of mean and RMS components as well as the mean temperature field using thermocouple data. The time response of the thermocouple was not sufficient to provide RMS temperature data.

Measurements are performed in transverse cuts and at the outlet of the diagonal swirler as represented in Fig. 6. For the cold flow, data are gathered over 15 cuts ranging from $x/R = 0.37$ to $x/R = 4.17$, where R is the radius of the burner outlet. For the case with combustion, there are six cuts ranging from $x/R = 0.7$ to $x/R = 4.32$.

7. Inlet conditions

A major issue in LES calculations is to specify boundary conditions. Since the axial swirler is fully computed, the flow is introduced before the vanes in section A (Fig. 6) without swirl and the computation should produce the right flow field at the burner mouth. The main problem is then to specify inlet conditions for the diagonal swirler (section D in Fig. 6). Section D is located at the trailing edge of the vanes of the diagonal swirler and velocities could not be measured at this location. The LES, however, starts in section D, and the inlet velocity profiles in this section are adjusted to match the first measurement section (cut 1d in Fig. 6) in the burner under nonreacting cases.

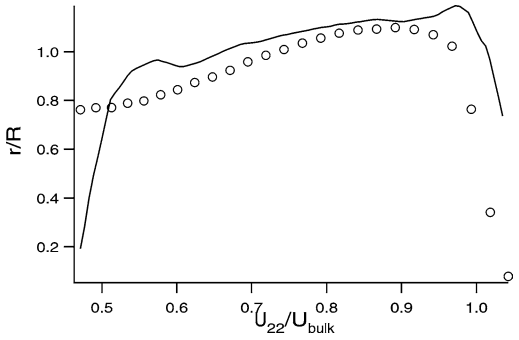

Fig. 7. Normalized velocity U_{22}/U_{bulk} at the exit of the diagonal swirler (cut 1d in Fig. 6).

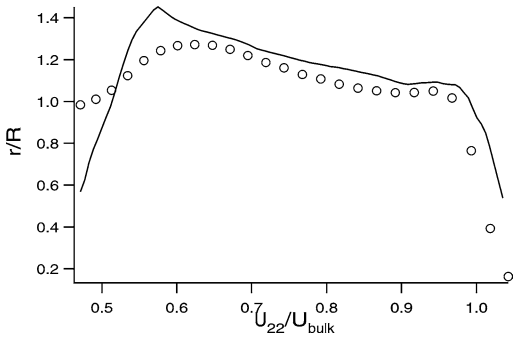

Fig. 8. Normalized swirl velocity W/U_{bulk} at the exit of the diagonal swirler (cut 1d in Fig. 6).

Velocity measurements have been performed in various sections displayed in Fig. 6. The swirling velocity W and the velocity U_{22} normal to a plane parallel to the diagonal swirler exit plane (at an angle of 22° compared with the vertical axis) are measured in the test section located close to the burner nozzle (cut 1d). Distances and velocities are respectively scaled by the burner radius R, and the bulk velocity U_{bulk} is defined by $U_{\text{bulk}} = \dot{V}/\pi R^2$, where $\dot{V}$ is the total volume flow rate through the burner.

Average profiles of axial and tangential velocities at the exit of the diagonal burner are displayed in Figs. 7 and 8 (cut 1d in Fig. 6). In figures, symbols denote experimental data while LES results are plotted with solid lines. No fluctuating velocity components are added to the inlet conditions: this incoming turbulence can be neglected compared with the turbulent activity in the chamber, which is due to the very high velocity gradients created by the swirling motion in the dump plane of the chamber. This is confirmed in the next section by the comparison of experimental and computational fluctuating velocity components in the chamber.

8. Nonreacting flow results

8.1. Averaged fields

Once the inlet conditions have been set, LDV measurements (○) are compared with averaged LES results (—) at different downstream locations x in the combustor (Fig. 9–12). In Fig. 9 (axial velocity profiles) and Fig. 10 (swirling velocities), LES data are averaged over 36 ms, corresponding to two flow times through the entire combustion chamber at the bulk velocity. Only 6 downstream locations are displayed for clarity, but 15 were investigated.

The agreement between LES and experimental data is excellent. The size, shape, and intensity of the recirculation zone are well predicted, as is the overall spreading of the turbulent swirling jet. All results are displayed for the whole size of the combustion chamber and not only for one half chamber to evidence symmetry defaults. As the chamber is square and the injection device axisymmetric, average velocities are expected to be symmetrical versus the x axis. However, both experimental data and LES results are not perfectly symmetrical, especially downstream. This finding (which is quite usual in these flows) may indicate a lack of sampling of LES data, but may also be due to an intrinsic difficulty in such flows to follow the symmetry of the geometry.

Concerning the RMS profiles (Figs. 11 and 12), only the resolved part of the fluctuations is taken into account here. This demonstrates that for this flow, most of the unsteady motion lies in large structures which are very well predicted by LES methods. Cut $x/R = 0.37$ in Fig. 12 shows that the largest fluctuations of the swirling component are located on the axis, and reach up to 60% of the bulk velocity. This is explained in the following subsection by the presence of a coherent structure.

An additional quantity that can be extracted directly from this compressible LES is the RMS pressure P', both in the chamber and on its walls. Fig. 13 shows that the largest pressure oscillations are found in front of the axial swirler outlet. Fairly high pressure levels (2500 Pa) are observed inside the combustor at the swirler outlet but they do not propagate to the walls. Most of these pressure oscillations are due to the precessing vortex described in the next subsection.

8.2. Unsteady flow analysis

Swirling flows can exhibit a very large range of topologies, depending mainly on the swirl number (see the review on vortex breakdown in [35]). For high values of the swirl number, the central recirculation zone may oscillate at a given frequency. This phenomenon is often referred to as precessing vortex core (PVC): the vortex aligned with the axis of

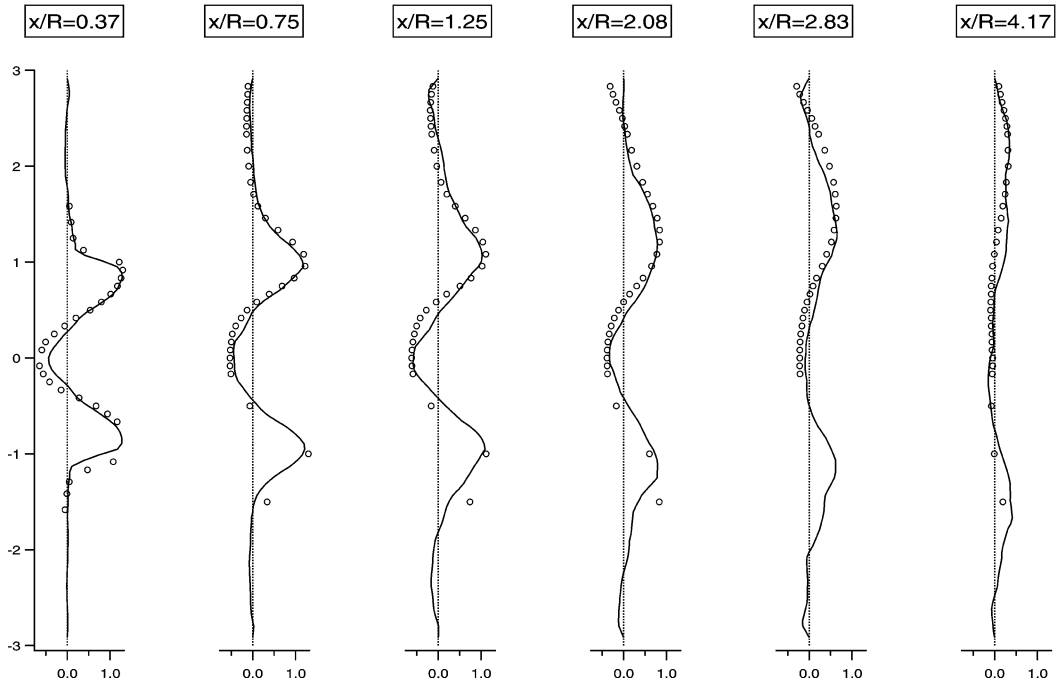

Fig. 9. Cold flow validation: mean axial velocity U/U_{bulk}.

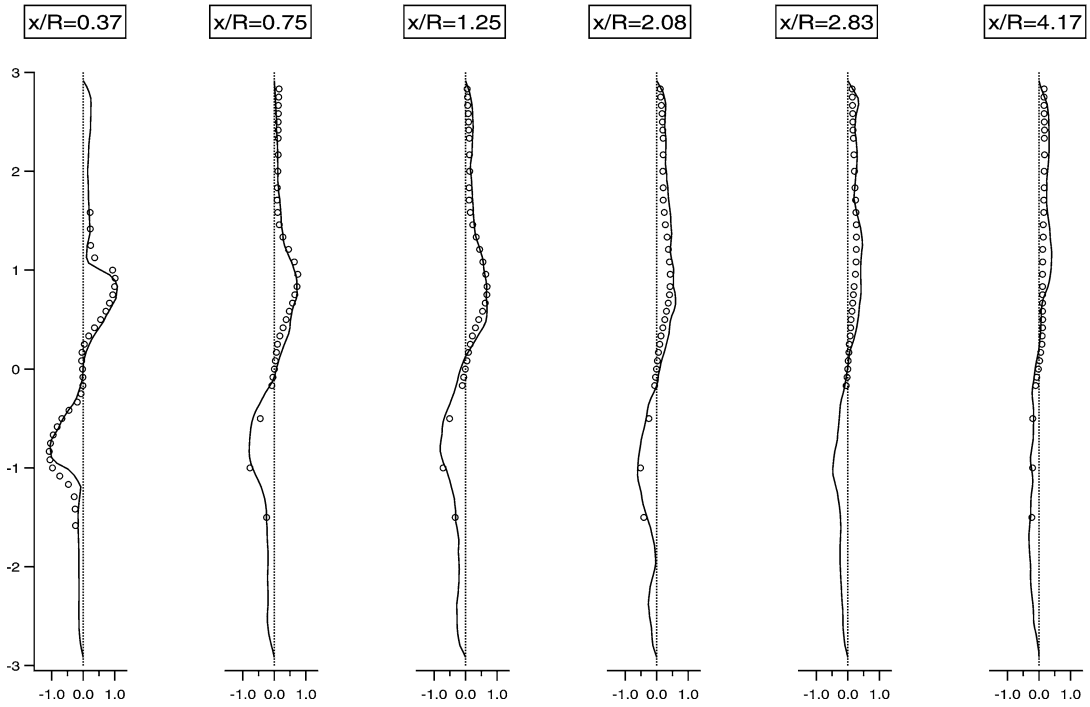

Fig. 10. Cold flow validation: mean swirling velocity W/U_{bulk}.

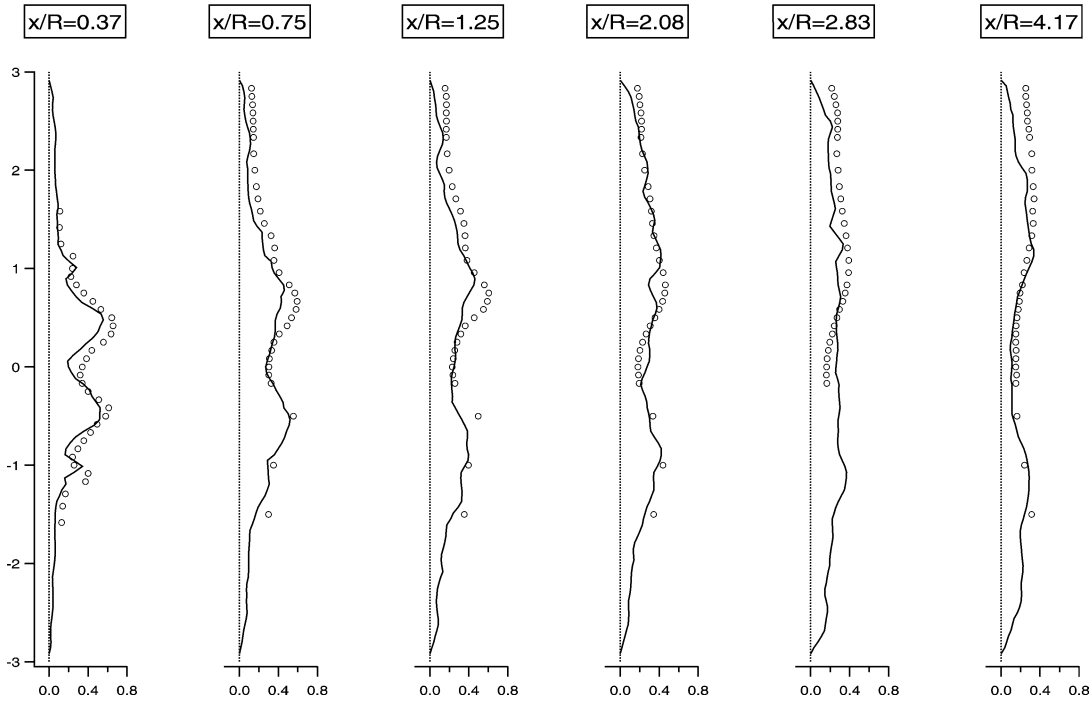

Fig. 11. Cold flow validation: axial velocity fluctuations U'/U_{bulk}.

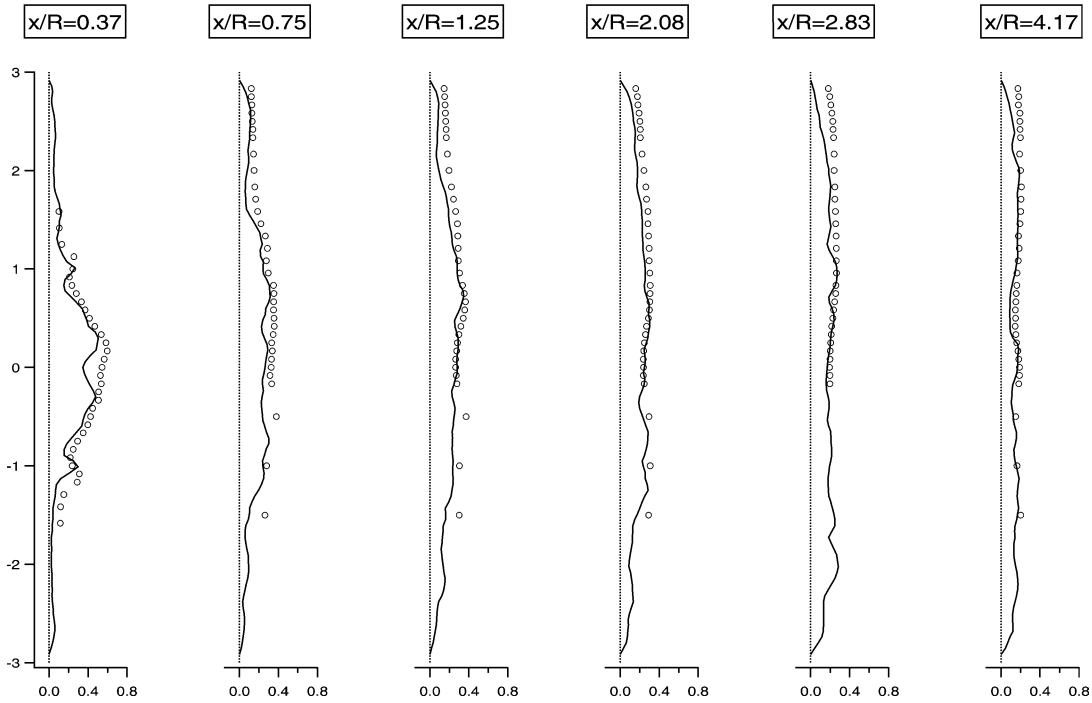

Fig. 12. Cold flow validation: swirling velocity fluctuations W'/U_{bulk}.

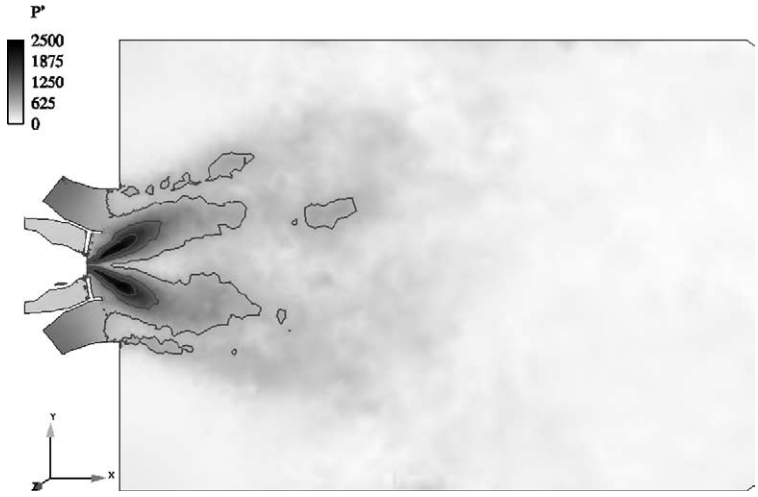

Fig. 13. RMS pressure fluctuations P' in a longitudinal cut for the cold flow (Pa).

the chamber (due to the swirl) breaks down in a spiral form. In the present regime, the flow inside the spiral is recirculated. The entire structure rotates around the axis of the chamber, causing large perturbations. The present LES captures this phenomenon: on the burner axis, at point A1 (Fig. 6), the velocity component W oscillates with time (Fig. 14) at a frequency $f_{\text{LES}} = 275$ Hz (Fig. 15). Indeed, if the flow were axisymmetric, W would be zero on the axis of the burner. The computed Strouhal number $St = (2Rf_{\text{LES}})/U_{\text{bulk}} = 0.63$ is typical of swirling flows [36]. The value of f_{LES} is also very close to that obtained experimentally at ITS: $f_{\text{exp}} = 255$ Hz.

Note that the LES gives additional information on the temporal evolution of the PVC: the sense of rotation of the whole spiral, as a structure, is that of the surrounding swirling flow, but the sense of winding of this spiral is opposite to that of the swirl. Fig. 16 is an instantaneous visualization of the PVC in the cold flow.

9. Reacting flow results

Reacting cases are computed starting from a cold flow solution. Fresh premixed gases (equivalence ratio $\phi = 0.5$) are injected through the diagonal swirler. The axial and diagonal flows, coming from the compressor in the actual gas turbine, enter the combustion chamber of the ITS burner after being preheated electrically to a temperature $T = 673$ K. As the actual ignition process is not described here, the chemical reaction is numerically started by filling the combustion chamber with hot fully burned gases. Note, however, that the pressure increases by 25% and the Mach number goes up to 0.4 in the outlet contraction during the transient ignition phase [33].

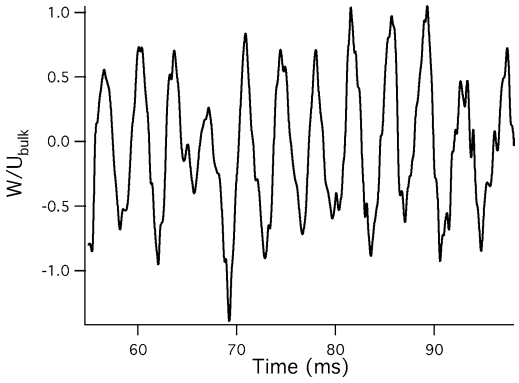

Fig. 14. Cold flow: W velocity at point A1 (see Fig. 6).

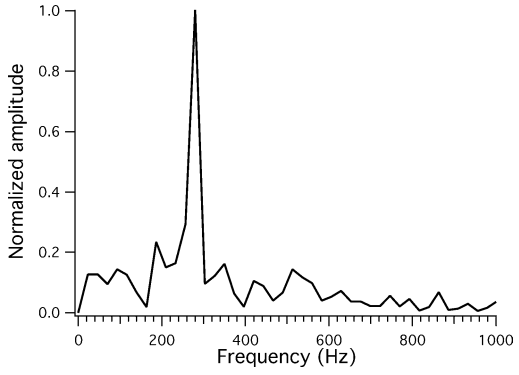

Fig. 15. Cold flow: Fourier transform of W velocity signal at point A1 (Fig. 6).

9.1. Unsteady flow analysis

A three-dimensional visualization of the reacting flow field is displayed in Fig. 17: the temperature iso-surface at $T = 1000$ K shows the geometry of the flame surface and illustrates the turbulent nature of the flame/flow interaction. Pockets of fresh gases are periodically shed from the main flame zone and burn downstream. A central core of hot gases is stabilized along the burner axis by the recirculation zone induced by swirl: this core is attached to the face of the axial swirler (Fig. 18). The field of axial velocity, normalized by U_{bulk}, is displayed in Fig. 19 with isocontours of heat release.

A specific feature of the reacting case is that the PVC structure evidenced in the cold flow cases disappears when combustion is turned on. Fig. 20 is a record of the velocity in the horizontal central plane (W) at point A1 (Fig. 6) after ignition. The velocity signal oscillates around zero as the core of the recirculation zone moves around the axis of the combustion chamber. After a few periods, the PVC motion vanishes. This observation obtained from LES data is confirmed by experimental results.

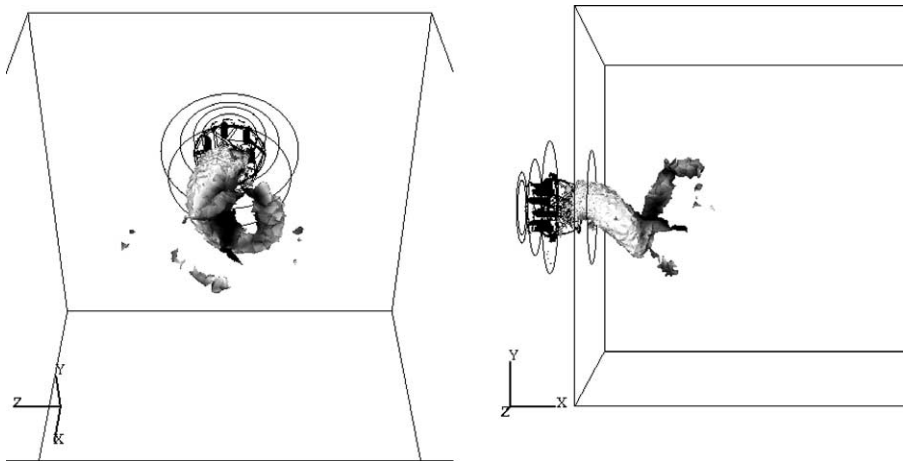

Fig. 16. Visualization of the PVC structure in the LES by a pressure iso-surface.

9.2. Averaged fields

In this section, the mean results of the LES (—) are compared with experimental data (○). Figs. 21–25 show the measurements conducted only in one-half of the combustion chamber.

Mean temperature profiles obtained from LES are compared with experimental data in Fig. 21. The agreement between LES and experimental data is good, and quantities that are important for the turbine design are well reproduced:

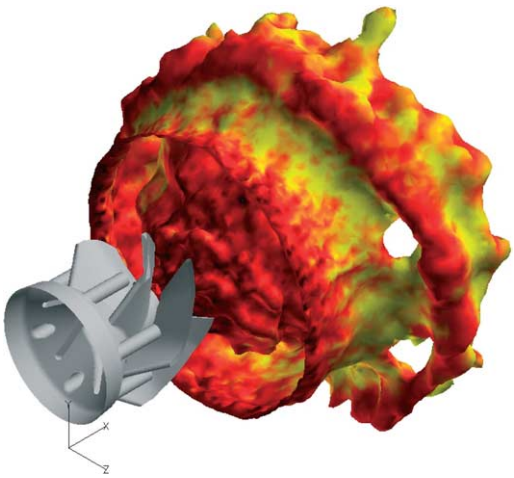

Fig. 17. Axial swirler vanes and temperature iso-surface ($T = 1000$ K) colored by velocity modulus.

- The angle, thickness, and length of the turbulent flame brush are very well predicted.
- The burnt gas temperature is very slightly overpredicted by the LES, mainly due to the nonadiabaticity of the experiment, while the LES assumes adiabatic walls.

Mean axial and tangential velocity profiles are respectively given in Figs. 22 and 23. The agreement is good: the size and intensity of the recirculation zone are very well predicted. The LES accurately captures the drastic increase in the angle of the jet compared with the cold flow (Fig. 9). RMS profiles of both axial and tangential velocities are plotted in Figs. 24 and 25. The level of the fluctuations is well predicted. Though the shape and level of axial velocity RMS fluctuations have not changed significantly between cold and hot flow (Figs. 11 and 24), swirling velocity RMS fluctuations are very different on the first profiles (Figs. 12 and 25). At $x/R = 0.37$, for example, the RMS swirling speed is $W'/U_{\text{bulk}} \simeq 0.7$ on the burner axis ($y = 0$) in Fig. 12 for the cold flow, and it decreases to $W'/U_{\text{bulk}} \simeq 0.1$ in Fig. 25 with combustion. This confirms that the fluctuations of azimuthal component are strongly reduced with combustion due to the suppression of the PVC structure, and the LES captures this effect with accuracy.

Analysis of the pressure fluctuations P' in a longitudinal cut reveals another important difference between cold and reacting flows: the pressure fluctuations observed in the cold flow (see Fig. 13) in front of

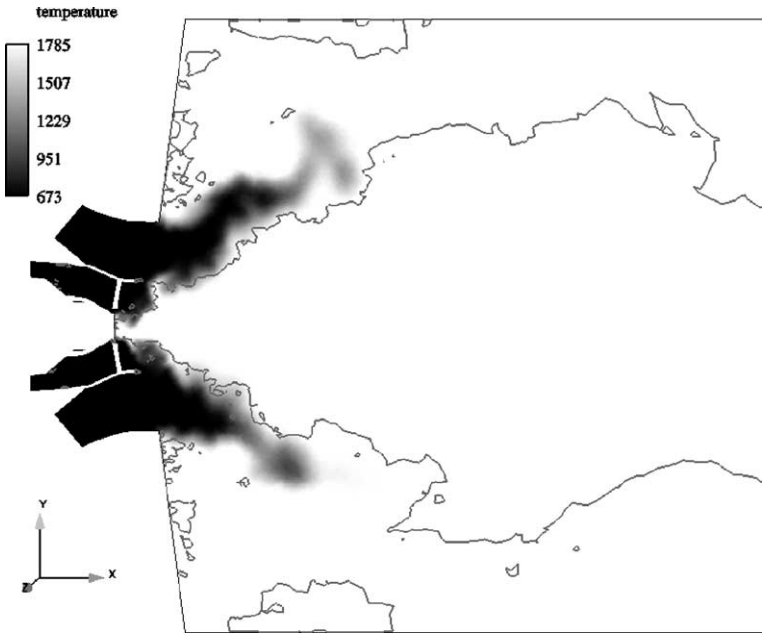

Fig. 18. Instantaneous temperature field and contour of zero axial velocity in a longitudinal cut of the burner.

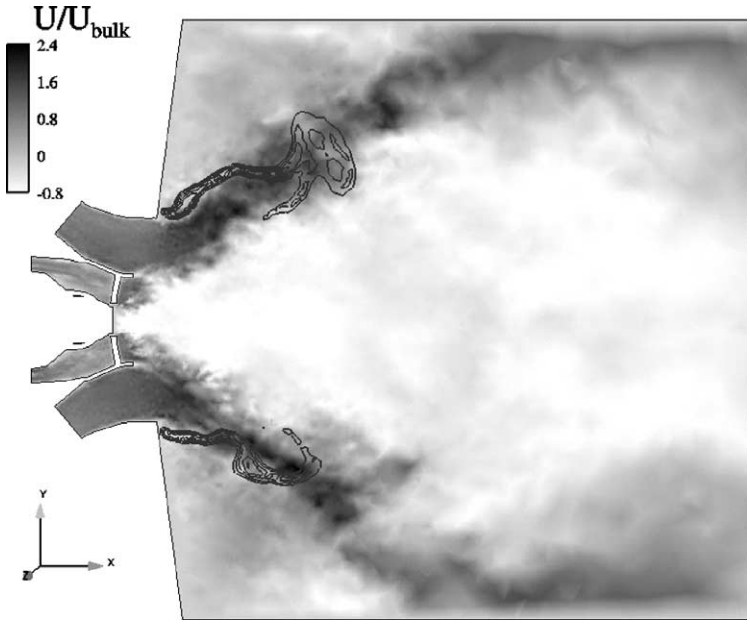

Fig. 19. Instantaneous axial velocity field and contours of reaction rate in a longitudinal cut of the burner.

the axial swirler disappear when combustion is turned on (Fig. 26). This is consistent with the suppression of the PVC when combustion is started: the cold flow unsteady pressure field is dominated by the presence of the PVC, while the reacting flow inhibits the PVC. The pressure field structure with combustion (Fig. 26) corresponds to an acoustic mode of the chamber [37] which is not analyzed in this paper.

10. Conclusions

A computation of a full burner of a premixed gas turbine installed in a laboratory rig was performed using LES for both nonreacting and reacting cases. The flame is described using a two-step chemical scheme for methane/air combustion combined with the Thickened Flame model. LES results are validated from velocity and temperature measurements performed at the University of Karlsruhe. The overall agreement with experiment is very good both for cold flow and for reacting conditions. A strong precessing vortex core is observed for the nonreacting flow. This vortex disappears when combustion is activated in both the experiment and the LES. Unsteady pressure fields are also very different for cold and reacting flow: maximum pressure oscillations are observed in the PVC zone for the cold flow; with combustion, the pressure oscillation maxima are located at the chamber walls and have an acoustic structure corresponding to a transverse-longitudinal mode, which is not studied in this paper. More generally, this study demonstrated that LES for reacting flows in complex geometries has now reached sufficient maturity to bring original information on such complex combustion devices.

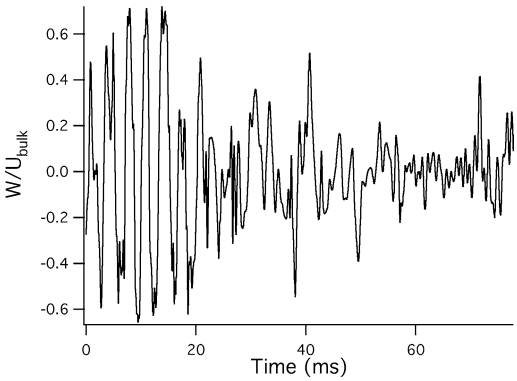

Fig. 20. Reacting flow: *W* velocity signal at point A1 (see Fig. 6). The PVC evidenced in the cold flow vanishes after ignition.

Acknowledgments

Certain numerical simulations have been conducted on the computers of CINES and IDRIS French national computing centers. Part of this work was carried out during the 2002 Center for Turbulence Research Summer Program at Stanford.

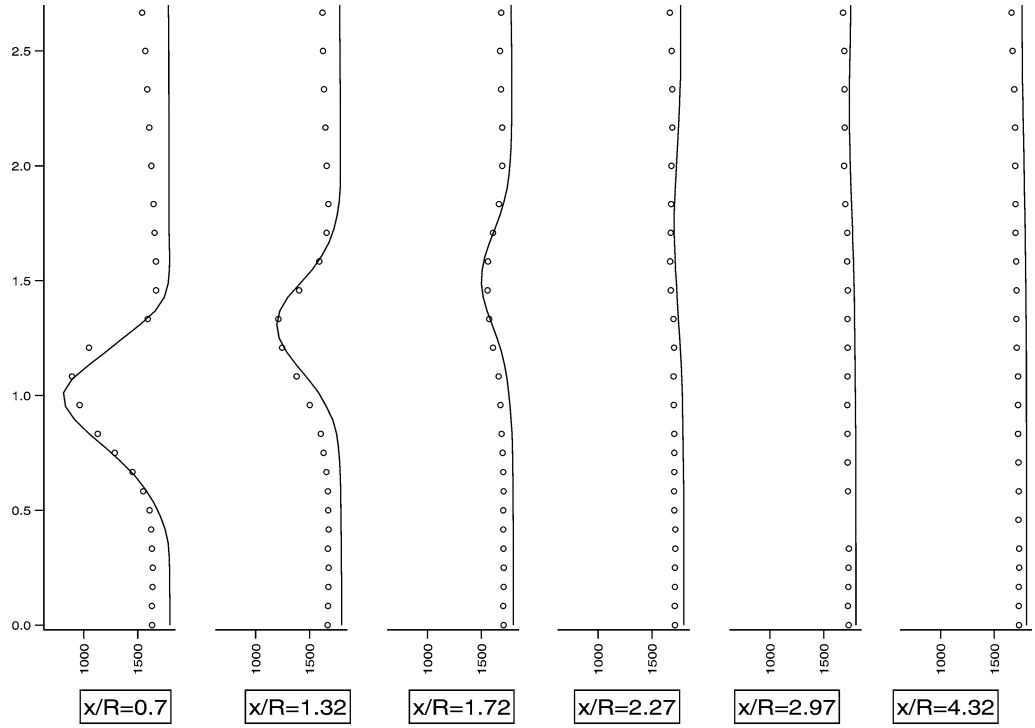

Fig. 21. Reacting flow validation: mean temperature (K).

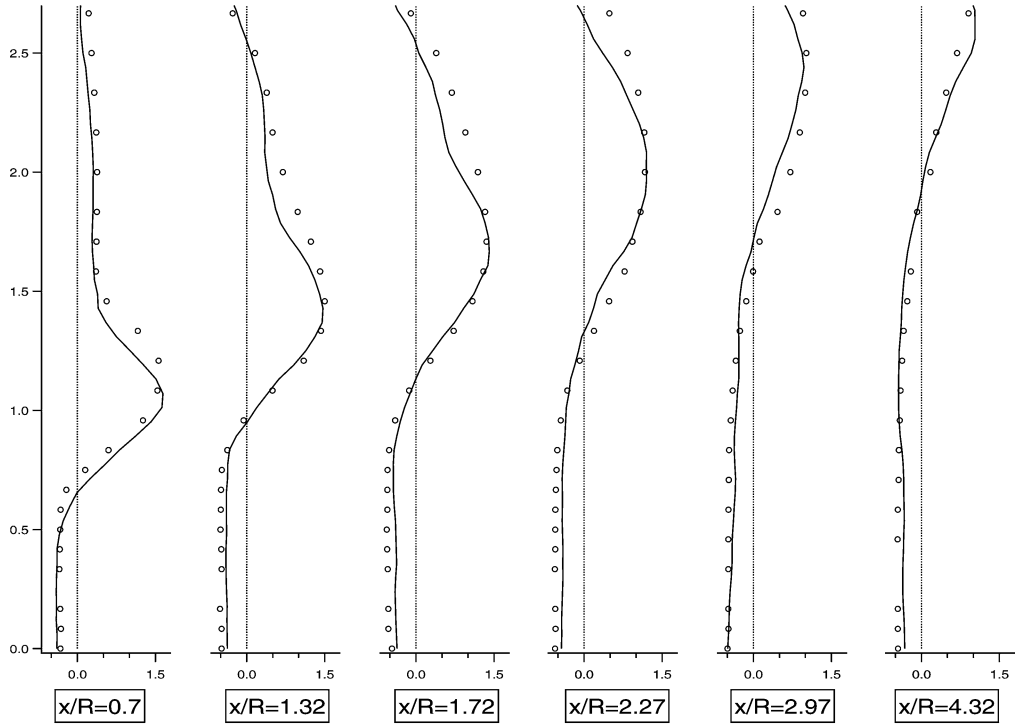

Fig. 22. Reacting flow validation: mean axial velocity U/U_{bulk}.

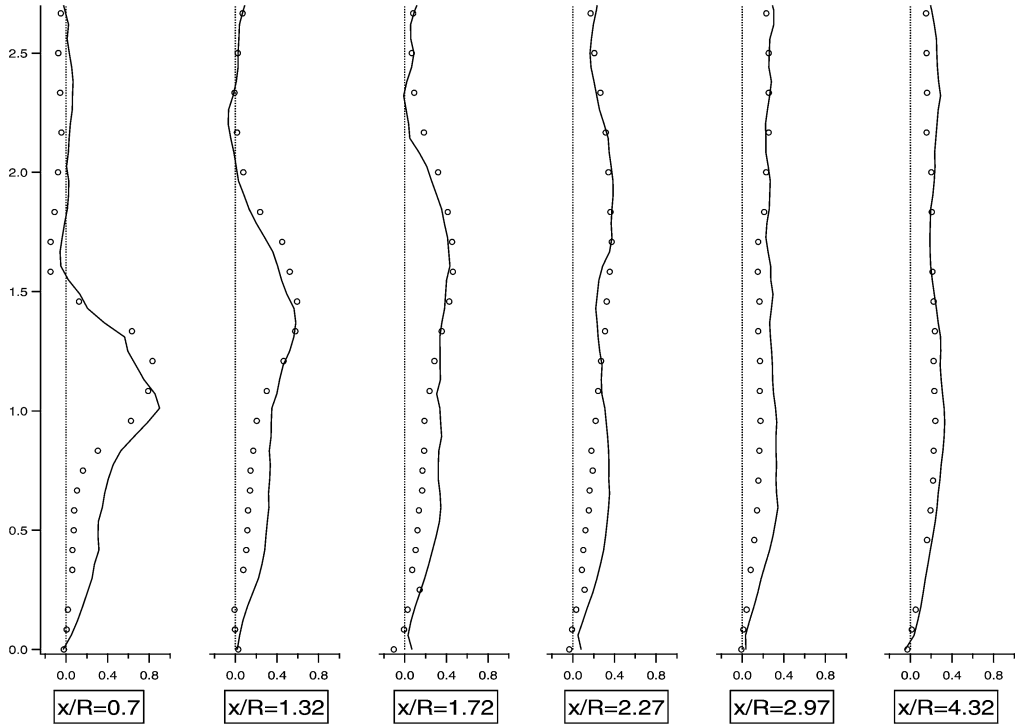

Fig. 23. Reacting flow validation: mean swirling velocity W/U_{bulk}.

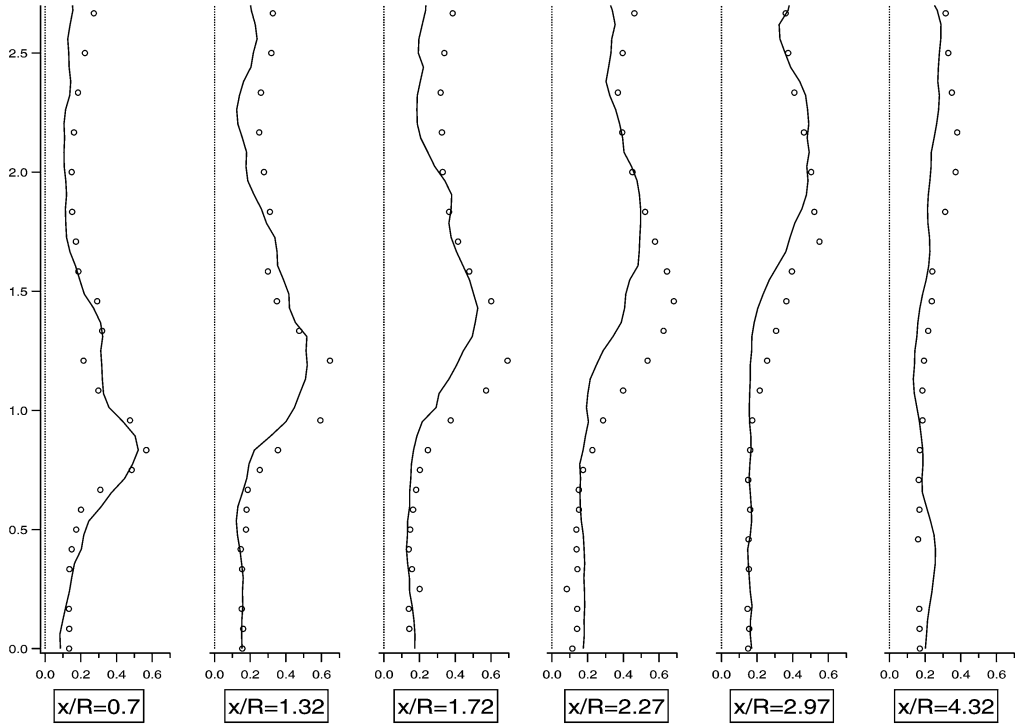

Fig. 24. Reacting flow validation: axial velocity fluctuations U'/U_{bulk}.

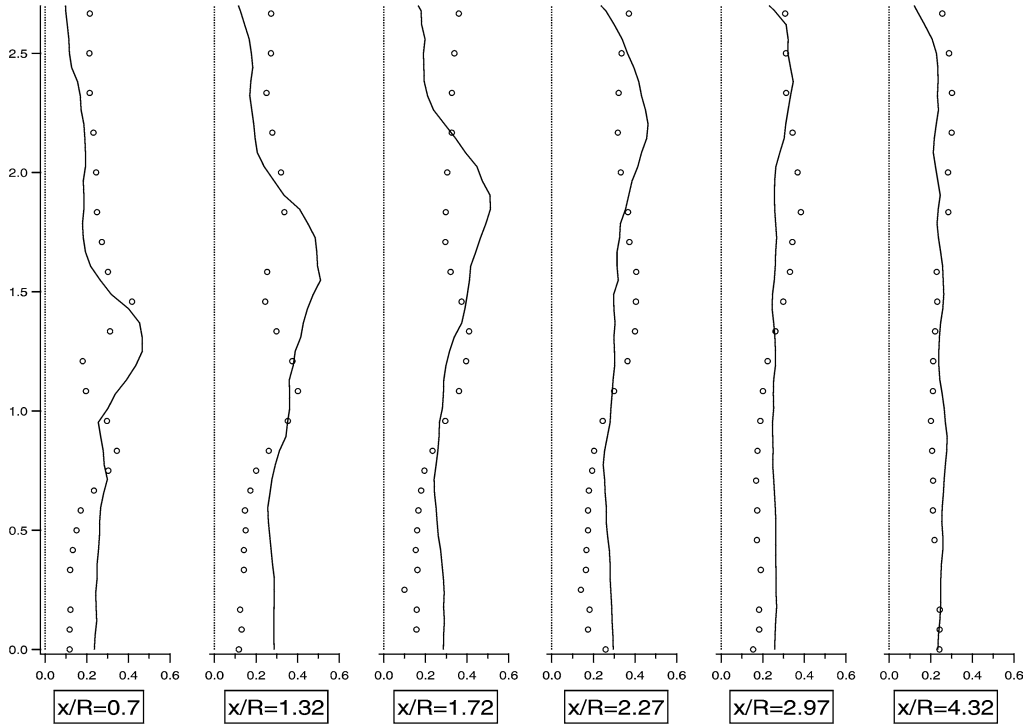

Fig. 25. Reacting flow validation: swirling velocity fluctuations W'/U_{bulk}.

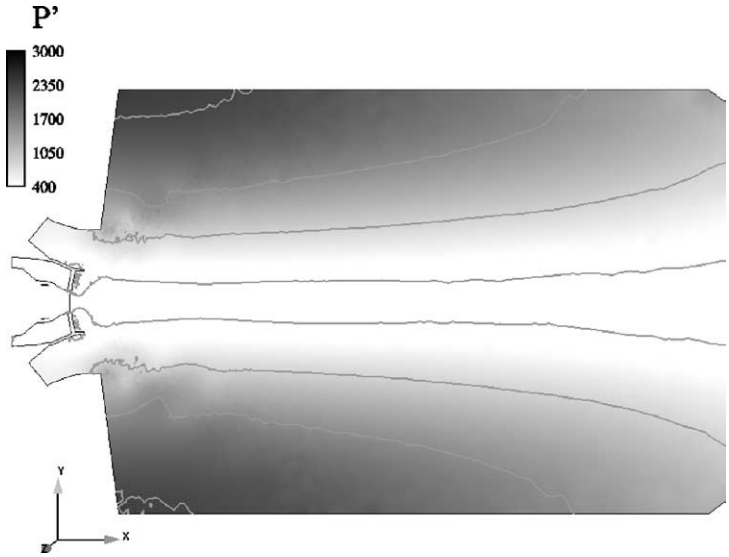

Fig. 26. RMS pressure fluctuations P' in a longitudinal cut for the hot flow (Pa).

References

[1] N. Peters, Turbulent Combustion, Cambridge Univ. Press, London/New York, 2000.
[2] T. Poinsot, D. Veynante, Theoretical and Numerical Combustion, R.T. Edwards, Flourtown, PA, 2001.
[3] C. Angelberger, F. Egolfopoulos, D. Veynante, Flow Turb. Combust. 65 (2000) 205–222.
[4] D. Caraeni, C. Bergström, L. Fuchs, Flow Turb. Combust. 65 (2000) 223–244.
[5] O. Colin, F. Ducros, D. Veynante, T. Poinsot, Phys. Fluids 12 (2000) 1843–1863.

[6] P.E. Desjardins, S.H. Frankel, Combust. Flame 119 (1999) 121–133.
[7] J.-P. Légier, T. Poinsot, D. Veynante, in: Proceedings, Summer Program, Center for Turbulence Research, NASA Ames/Stanford Univ., Stanford, CA, 2000, pp. 157–168.
[8] C.D. Pierce, P. Moin, in: 29th Fluid Dynamics Conference, Albuquerque, NM, 1998.
[9] H. Pitsch, L. Duchamp de la Geneste, Proc. Combust. Inst. (2002) 2001–2008.
[10] L. Duchamp de Lageneste, H. Pitsch, CTR Annual Research Briefs (2001) 61–82.
[11] A. Kempf, H. Forkel, J.-Y. Chen, A. Sadiki, J. Janicka, Proc. Combust. Inst. (2000) 35–40.
[12] H. Pitsch, H. Steiner, Proc. Combust. Inst. (2000) 41–49.
[13] P. Sagaut, Large Eddy Simulation for Incompressible Flows, Springer-Verlag, Berlin/New York, 2000.
[14] A. Scotti, C. Meneveau, D.K. Lilly, Phys. Fluids 5 (1993) 2306–2308.
[15] A. Scotti, C. Meneveau, M. Fatica, Phys. Fluids 9 (1997) 1856–1858.
[16] O.V. Vasilyev, T.S. Lund, P. Moin, J. Comput. Phys. 146 (1998) 82–104.
[17] K. Mahesh, G. Constantinescu, S. Apte, G. Iaccarino, F. Ham, P. Moin, in: Annual Research Briefs, Center for Turbulence Research, NASA Ames/Stanford Univ., 2002, pp. 115–142.
[18] Combustion Research Facility Division at Sandia http://www.ca.sandia.gov/crf/index.html.
[19] CFD team at CERFACS http://www.cerfacs.fr/cfd/CFDWeb.html.
[20] F. Nicoud, F. Ducros, Flow Turb. Combust. 62 (1999) 183–200.
[21] D. Angelberger, D. Veynante, F. Egolfopoulos, T. Poinsot, in: Proceedings, Summer Program, Center for Turbulence Research, NASA Ames/Stanford Univ., 1998, pp. 61–82.
[22] J.-P. Légier, Simulations numériques des instabilités de combustion dans les foyers aéronautiques, PhD thesis, INP Toulouse, 2001.
[23] O. Colin, M. Rudgyard, J. Comput. Phys. 162 (2000) 338–371.
[24] T. Poinsot, S. Lele, J. Comput. Phys. 101 (1992) 104–129.
[25] M. Baum, T.J. Poinsot, D. Thévenin, J. Comput. Phys. 116 (1994) 247–261.
[26] H. Forkel, J. Janicka, Flow Turb. Combust. 65 (2000) 163–175.
[27] H. Pitsch, H. Steiner, Phys. Fluids 12 (2000) 2541–2554.
[28] V.K. Chakravarthy, S. Menon, Flow Turb. Combust. 65 (2000) 133–161.
[29] C. Fureby, S.I. Möller, AIAA J. 33 (1995) 2339.
[30] H.G. Weller, G. Tabor, A.D. Gosman, C. Fureby, Proc. Combust. Inst. 27 (1998) 899–907.
[31] T.D. Butler, P.J. O'Rourke, Proc. Combust. Inst. 16 (1977) 1503–1515.
[32] F. Charlette, D. Veynante, C. Meneveau, Combust. Flame 131 (2002) 159–180.
[33] L. Selle, G. Lartigue, T. Poinsot, P. Kaufman, W. Krebs, D. Veynante, in: Proceedings, Summer Program, Center for Turbulence Research, Stanford Univ./NASA–Ames, 2002, pp. 333–344.
[34] W.P. Jones, R.P. Lindstedt, Combust. Flame 73 (1988) 222–233.
[35] O. Lucca-Negro, T. O'Doherty, Prog. Energy Combust. Sci. 27 (2001) 431–481.
[36] A.K. Gupta, D.G. Lilley, N. Syred, Swirl Flows, Abacus Press, 1984.
[37] L. Selle, Simulation aux grandes échelles des interactions flamme/acoustique dans un écoulement vrillé, PhD thesis, INP, 2004.